Ultrasonics 89 (2018) 26–33

Contents lists available at ScienceDirect

Ultrasonics

journal homepage: www.elsevier.com/locate/ultras

Effects of ultrasonic vibration on the compression of pure titanium

Tao Liu, Jun Lin*, Yanjin Guan, Zhendong Xie, Lihua Zhu, Jiqiang Zhai

Key Laboratory for Liquid-Solid Structural Evolution & Processing of Materials (Ministry of Education), Shandong University, Jinan 250061, China

ARTICLE INFO

Keywords:
Ultrasonic vibration
Softening
Pure titanium
Compression
Deformation mechanism

ABSTRACT

The technology of ultrasonic vibration assisted plastic forming possesses a great many merits, such as reducing the deformation resistance and friction, as well as improving the surface quality of parts. In this study, the ultrasonic vibration assisted compression tests were carried out on pure titanium in order to improve its formability. The results indicating that the ultrasonic vibration had no effort on elastic deformation, and the temperature of material only increased by 6 °C after compression with applying the ultrasonic vibration. Therefore the influence of temperature increase on reduction of flow stress could be ignored. After excluding interface friction and temperature effects, ultrasonic vibration can still decline the flow stress, the mechanism of deformation includes ultrasonic softening, stress superposition and strain hardening. In the intermittent vibration tests, the material shows the residual softening effect after stopping vibration. By observing the microstructure of material with SEM, it shows that the ultrasonic vibration can promote the generation of deformation twins, causing the grain refinement and the reduction of the twins, which is the major factor of affecting the residual softening effect.

1. Introduction

In recent years, Titanium and its alloys are widely used in aviation, spaceflight, electronics, transportation, medical, ocean engineering and other fields [1], because of its low density, high strength, good corrosion resistance, high temperature resistance and low temperature resistance, etc. [2] However, the plastic forming ability of titanium and its alloy is low and the springback problem is always accompanied at room temperature [3]. In addition, it is difficult to form parts with complex shapes. Therefore, at present the forming process of titanium and its alloys is mainly performed in hot state [4], including vacuum creep forming and superplastic forming, etc. However, in this procedure the titanium and its alloy are easy to be oxidized and worn under high temperature, and also the problems such as heating equipment and high temperature resistant mould need to be taken into account. As we all know, ultrasonic vibration assisted plastic forming technology is a novel technology risen in the past two decades. It can reduce the deformation resistance and friction [5], and improve the surface quality of parts together with the material formability, resulting in a special characteristic to forming the materials with high strength and low plasticity [6]. Therefore, the application of ultrasonic vibration assisted plastic forming technology to titanium alloy can improve the forming ability of titanium alloy, which will further promote the development and application of titanium and its alloy products.

As early as 1955, Blaha and Langenecker [7] found in zinc bar tensile test with applying ultrasonic vibration, that the material was "softened", namely the forming force was reduced. This phenomenon is called as "Blaha" phenomenon afterwards. Nowadays, ultrasonic vibration has been widely used in plastic forming processing, such as tension [8], compression [9], drawing [10], spinning [11], incremental forming [12], extrusion [13], equal channel angular pressing [14], micro-upsetting [15] and so on for aluminum and copper alloys. Yet in recent three years, ultrasonic vibration assisted forming technologies for titanium and its alloys have attracted much attention and become to be a research hotspot.

At present, Fartashvand et al. [16] studied the influence of high power ultrasonic vibration on powder compaction forming of pure titanium. Under the effect of ultrasonic vibration, the density of titanium compacts with initial particle size < 45 μm was increased by 7.53% and the fine particle powder showed good consolidation effect. Furthermore, the friction stress was reduced up to 88.5% in fine powders. They [17] also studied the acoustic softening effect of TC4 titanium alloy in ultrasonic vibration assisted tension test. The study showed that the yield stress and ultimate stress of the materials under ultrasonic power were reduced, and the elongation rate was increased up to 13%. In addition, there was no significant temperature rise was observed. Yang et al. [18] imposed the longitudinal-torsional composite ultrasonic vibration on the influence of titanium wire drawing process. They found that both the longitudinal vibration and the longitudinal-torsional composite vibration were beneficial to decreasing the drawing force

* Corresponding author.
E-mail address: linjun@sdu.edu.cn (J. Lin).

https://doi.org/10.1016/j.ultras.2018.04.006
Received 9 February 2018; Received in revised form 2 April 2018; Accepted 22 April 2018
Available online 24 April 2018

and improving the plasticity of titanium wires, especially for the latter. Longitudinal-torsional composite ultrasonic vibration induced more elastic and plastic deformation and thus reduced the drawing force, but meanwhile caused the friction force to rise up slightly, making the surface quality worse. Zhao et al. [19] studied the effect of ultrasonic vibration frequency on surface deformation in rotary ultrasonic roller burnishing TC4 alloy. The result showed that ultrasonic vibration assisted rolling could reduce the flow stress of material which caused the decrease of burnishing force, and refine the grain surface of the material to reach the effect of strengthen. Zhou et al. [20] performed the ultrasonic vibration assisted compression tests of ERTA1ELI pure titanium. Under the effect of ultrasonic vibration, the flow stress decreased significantly. The initial residual hardening effect transformed into the residual softening effect with the increase of ultrasonic amplitude.

Although ultrasonic vibration technology has been developed for decades, its application in titanium and its alloys is not much studied [21], the roles of superposition of stress, softening effect, temperature increase and interface friction reduction played in the decline of flow stress in ultrasonic vibration assisted forming technology for titanium ally is complex and not clear [22]. The effect of the interface friction between the specimen and the tool head, as well as the compliances of the forming machine and the ultrasonic vibration device on the flow stress is rarely considered. Therefore, in this paper, the ultrasonic vibration assisted compression test of TA1 pure titanium column is carried out to study the influence of the ultrasonic vibration on the flow stress and further the deformation mechanism. In the compression process, the change of temperature of specimen was detected. Then the deformation of the specimen was calibrated by subtracting the deformation of the shaping tools from the recorded data. Meanwhile, the influence of interface friction between the specimen and the die was eliminated through an extrapolated compression test.

2. Ultrasonic vibration assisted compression test

2.1. Materials and specimen

Pure titanium (TA1) bar was used in this study, and its chemical composition was shown in Table 1. The titanium bar was manufactured according to the standard of GB/T 2965-2007 with a diameter of 5.0 mm and machined to the cylindrical specimen with a height of 3.75 mm, 5 mm, 6.25 mm and 7.5 mm respectively in the axial direction (the corresponding ratios of initial diameter to height D/H were 1.33, 1, 0.8 and 0.67), as shown in Fig. 1. Additional 0.2 mm height allowance was reserved in the original specimen for the surface grinding before the experiment. The specimen was annealed (kept at 600 °C for 2 h and then cooled in the furnace) to eliminate the residual stress caused by machining process. Finally, the surface of the annealed specimen was smoothed out with SiC sandpaper, and polished to the pre-described height.

2.2. Experimental procedure

The compression test was performed on a SANS CMT5205 universal testing machine at the room temperature of 30 °C, and the ultrasonic vibration device was assembled on the universal testing machine as shown in Fig. 2. The maximum compression force of the universal testing machine is 200 kN, and the range of crosshead beam moving speed is 0.001–250 mm/min, as well as the maximum stroke is 1100 mm. Ultrasonic vibration device consists of ultrasonic generator, transducer, horn and tool head [23]. The ultrasonic generator translates the alternating current into an ultrasonic electroshock signal. Then the transducer converts the high frequency electroshock signal into mechanical vibration, and the horn amplifies the ultrasonic amplitude. Eventually the ultrasonic vibration acts on the specimen through the tool head [24]. The frequency of the ultrasonic vibration device is 20 kHz, and the output amplitudes are 4.6 μm and 6 μm in the longitudinal direction corresponding to the power of 1600 W and 2000 W, respectively. In the compression test, the load is controlled by the crosshead moving speed.

Table 2 lists the process parameters employed in the ultrasonic vibration assisted compression test. The initial strain rate of the material is constant of 0.01 s^{-1} (the corresponding crosshead moving speed for bars of D/H 1.33, 1, 0.8 and 0.67 are 2.25 mm/min, 3 mm/min, 3.75 mm/min and 4.5 mm/min, respectively), The total compression amount is 50% of the specimen height, and each test repeated at least 3 times to ensure the accuracy of test results.

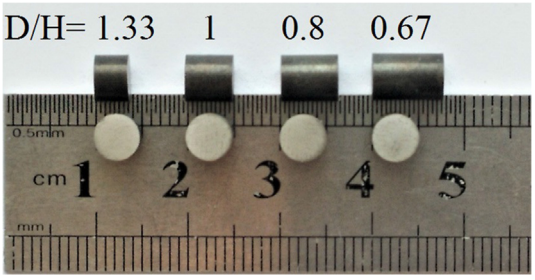

Fig. 1. Specimen of TA1 pure titanium for the compression test.

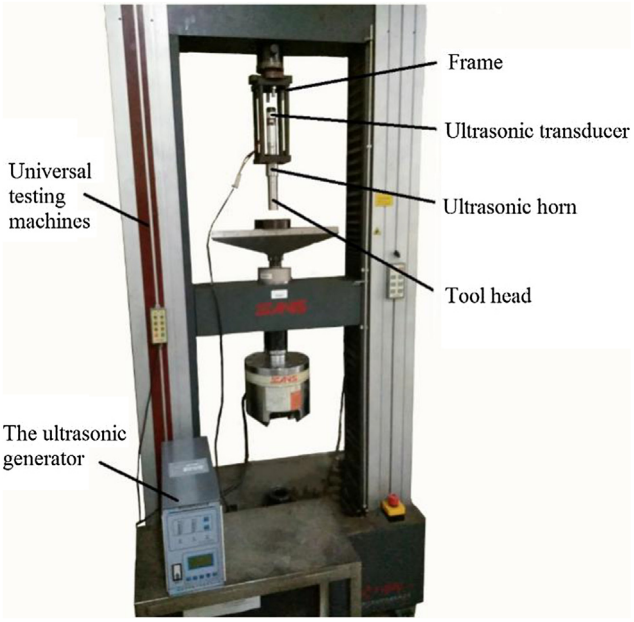

Fig. 2. Ultrasonic vibration assisted compression test equipment.

Table 1
The chemical composition of TA1 (%).

Ti	Fe	O	N	C	H
Balance	0.02	0.08	< 0.01	< 0.01	0.02

Table 2
The process parameters of compression test.

Vibrational frequency	20 kHz
Amplitudes	4.6 μm, 6 μm
Initial strain rate	0.01 s^{-1}
Amount of compression	50%
D/H ratios	0.67, 0.8, 1, 1.33
Vibration loading modes	Full vibration, intermittent vibration

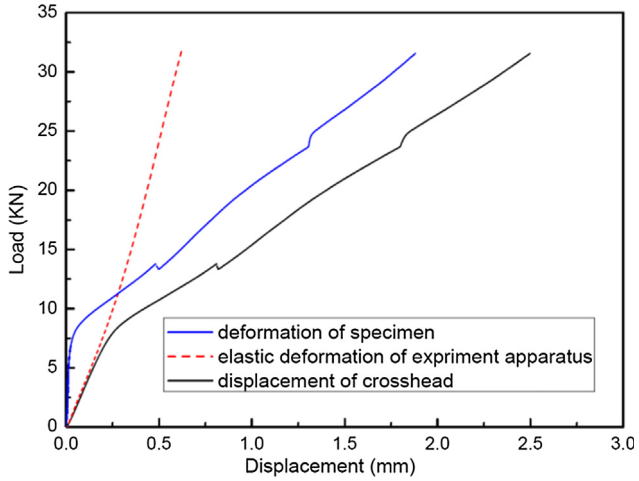

Fig. 3. Schematic of calibration of specimen deformation.

2.3. Calibration of the force-displacement curve

To eliminate the influence of the elastic deformation of the vibration device and the universal testing machine and then improve the accuracy of the force-displacement curve, the deformation of the specimen has to be calibrated. Firstly, the compression test without specimen was conducted, and the force and displacement data during the test were recorded, denoted as dotted line in Fig. 3. Then, the compression test with specimen was carried out to gain a novel force-displacement curve, shown as black solid line. The resulting actual deformation of the specimen is obtained by subtracting the displacement recorded in the compression test without specimen from one with specimen, shown as the black solid line. The calibrated force and displacement data were calculated and converted into engineering stress and engineering strain.

2.4. Frictionless treatment

Since the specimen is small, the friction between the tool and the specimen will affect greatly the stress-strain curve. Therefore, in order to remove the influence of the interface friction, a method named “the extrapolated compression test” proposed by Cook and Larke [25] was adopted to re-calculate the engineering stress-strain data. In this method, the authors considered that for the cylindrical specimens, when the diameter of specimens is constant under a compressive force, the interface friction will decrease with the increase of specimen height. That means when the height of the specimen is infinitely high, i.e. D/H ratio reaches 0, the interface friction can be ignored. To this aim, the compression tests of different D/H ratios (0.67, 0.8, 1.0, 1.33) were conducted to deduce the compression test data of infinite height specimen.

Fig. 4 plots the engineering strains corresponding to the different D/H ratios when the engineering stresses are 400 MPa, 800 MPa, 1200 MPa, and 1600 MPa (for case of conventional compression)/1520 MPa (for case of vibrated compression), respectively.

As shown in Fig. 4, the experimental compressive strains with regards to an identical load condition are nearly linear to the D/H ratios and can be extended to the origin point. The minimum correlation coefficients are −0.9577 and −0.9739 respectively for conventional and vibrated compression tests. The maximum relative error between the fitted curves and experimental values are 3.32% and 2.76%, respectively for conventional and vibrated compression tests.

Therefore by linear curve fitting, the intercepts can be got, which represent the engineering strains without friction influence when D/H = 0. The engineering stress-strain relationships with different D/H ratios are depicted in Fig. 5. Finally, these data were employed to compute the true stress-strain data. In fact, rather than 4 stress levels chosen in Fig. 4, 18 levels of engineering stress have been employed to extrapolate 18 strains at D/H = 0, to make the stress-strain curve for D/H = 0 smooth.

3. Experimental results and analysis

Fig. 6 shows the thermal image when ultrasonic vibration is stopped in the compression test. From the figure, the temperature of the specimen surface in contact with the tool head was highest, and the value was 36.4 °C, indicating that after the vibration was applied, the ultrasonic energy could be absorbed by the material and resulting in higher temperature. However, the temperature was only 6 °C higher than the room temperature, which could not cause a significant reduction of flow stress. Therefore, the influence of ultrasonic thermal softening on the test can be ignored.

Fig. 7 displays the true stress-strain curves at different D/H ratios. Fig. 7(a) shows the true stress-strain curves with no vibration at the D/H ratios of 0, 0.67, 0.8, 1 and 1.33. Fig. 7(b) and (c) are the true stress-strain curves under the vibration throughout the whole compression process and the amplitude is 4.6 μm and 6 μm, respectively. Taking into account that the specimen is easy to slip out of the work area if the high frequency vibration is applied at the beginning of the compression, a certain pre-pressure is needed to keep the specimen fixed in the working space before the application of ultrasonic vibration, which is set to be 1 kN in this study for the full vibration assisted compression tests.

To clearly observe the change for each loading mode, the true stress-strain values when the engineering stress is 1520 MPa are listed in Table 3. Comparing with the specimen of 1.33-D/H-ratio, the frictionless true stress decreased by 20.7%, 22.4% and 23.0% respectively, as well as the true strain increased by 64.9%, 65.3% and 65.6% respectively for the cases of conventional compression, vibrated compression with amplitudes of 4.6 μm and 6 μm. It can be concluded that under the same loading conditions, with the D/H decreases, the flow stress of the material decreases and the strain increases significantly. The reason is that the interface friction between the specimen and the die was reduced as the D/H decreases and energy dissipation gets small. In addition, the elastic modulus almost remains unchanged when applying the vibration throughout the whole compression, thus the impact of ultrasonic vibration on the plastic deformation is only taken into account in the following sections.

Fig. 8 shows the true stress-strain curves with different amplitudes under frictionless condition. In conventional compression, the yield stress of the material was 403 MPa. When the amplitude was 4.6 μm, the yield stress was 382 MPa, which has a decline of 21 MPa. And when the amplitude was 6 μm the yield stress was 372 MPa, with a decrease of 31 MPa compared to the conventional compression.

Obviously, ultrasonic vibration can reduce the yield stress of the material, making the material plastically formed in advance, and the more yield stress decreased with the amplitude increase. It also can be seen from Fig. 8 that when the strain reaches 0.59, the difference in true stress between the conventional and vibrated compressions and are −35.6 MPa and −46.7 MPa respectively for amplitude vibration of 4.6 μm and 6 μm. This demonstrates that when applying the vibration, the flow stress of the material can be reduced, and the magnitude of the decrease is approximately proportional to the amplitude.

In addition, one can observe from Fig. 8 that during the plastic deformation stage, the flow stress reduction between conventional compression and vibrated compression is increasing with the compression proceeds. According to the stress superposition mechanism, the mean stress of the material is decreased due to the repeated application and unloading of the force under the ultrasonic vibration condition [22], the path of the maximum oscillatory stress follows the path of the static stress–strain curve and that the path of the mean stress is lower than and parallel to the static stress–strain curve. Therefore, the decrease of average stress caused by stress superposition is of a

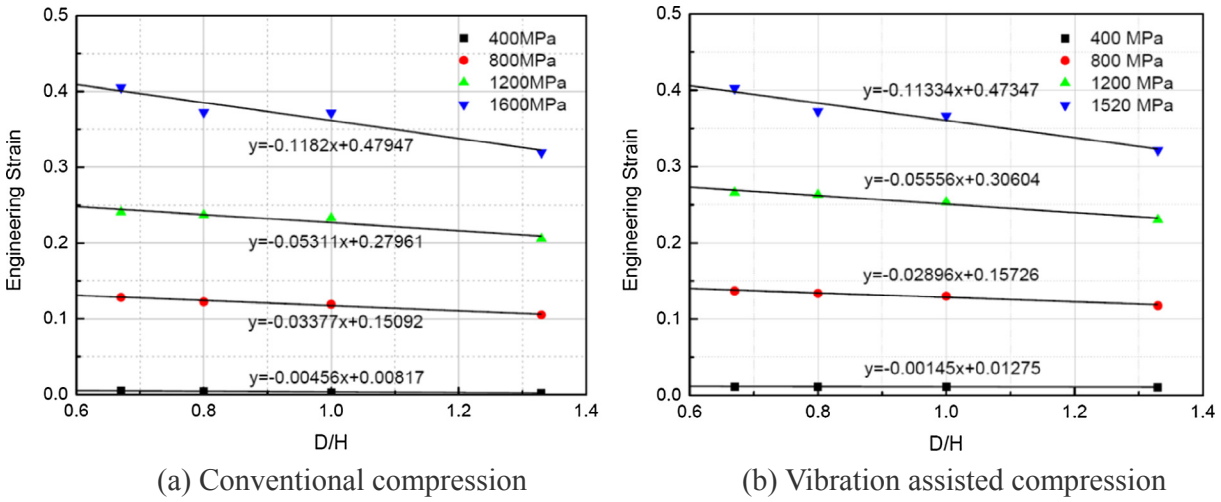

(a) Conventional compression (b) Vibration assisted compression

Fig. 4. Experimental to zero D/H for compressive strain.

certain value. Since the frictionless treatment was carried out in this study, there was no reduction in stress caused by the effect of friction reduction. Also, the thermal softening effect caused by ultrasonic vibration can also be neglected which mentioned above. Obviously, it is not feasible to explain the increasing stress reduction only by the effect of stress superposition. Therefore, there is acoustic softening effect in the ultrasonic vibration assisted compression under frictionless condition.

The true stress-strain curves after frictionless treatment in intermittent vibration assisted compression tests are shown in Fig. 9. In the compression process, the vibration began to be applied when the strain reached 0.11. As soon as the vibration was excited, it can be clearly seen that the stress had a significant decrease compared to the conventional compression experiment. When the stress reached the valley, the stress began to increase gradually as the strain increases and the path was almost parallel to the path with no vibration. After the ultrasonic vibration was terminated as strain reached 0.32, the stress of the specimen increased linearly with the strain increases, showing as an elastic deformation stage. And subsequently the material enters into plastic deformation stage again. These phenomena showed that the stress-reduction effect of ultrasonic vibration was contributed just in the period of the applied vibration. Finally, the flow stress recovered but less than the stress in case of no vibration. It indicates that the material had a residual softening effect, and this effect becomes larger as the amplitude increases. However, the residual hardening mentioned in

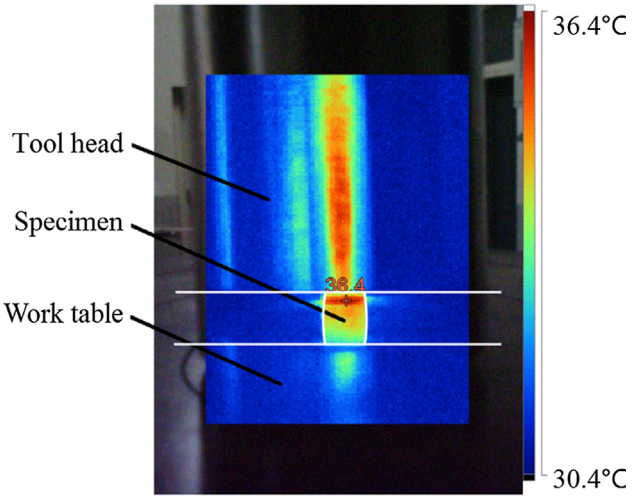

Fig. 6. Thermal image when ultrasonic vibration assisted compression.

Zhou [20] was not observed in this study, which might be due to the relatively long period of the applied ultrasonic vibration in present tests.

Fig. 10 depicts the true stress-strain curves of different vibration

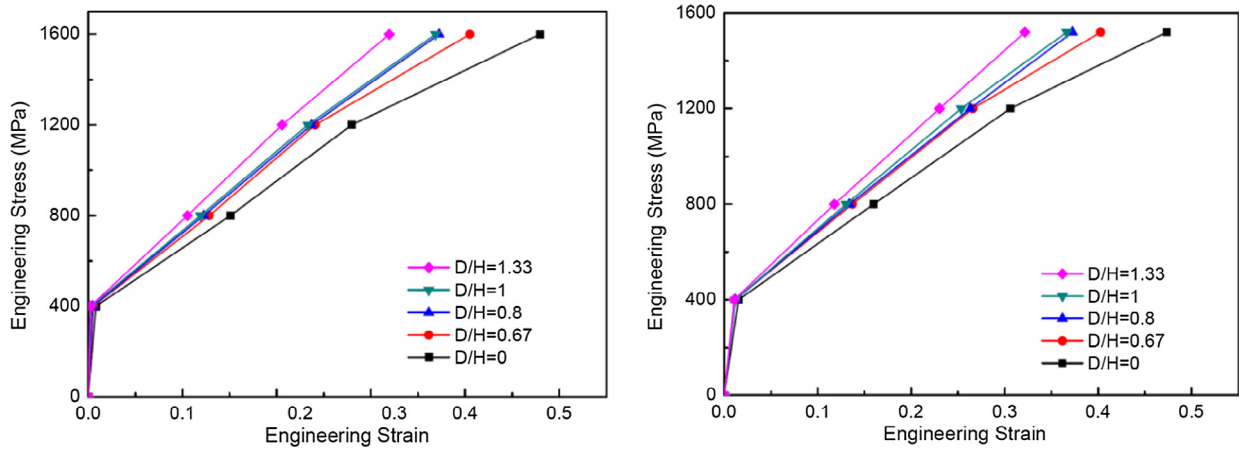

(a) Conventional compression (b) Vibration assisted compression

Fig. 5. Engineering stress-strain curves with different D/H.

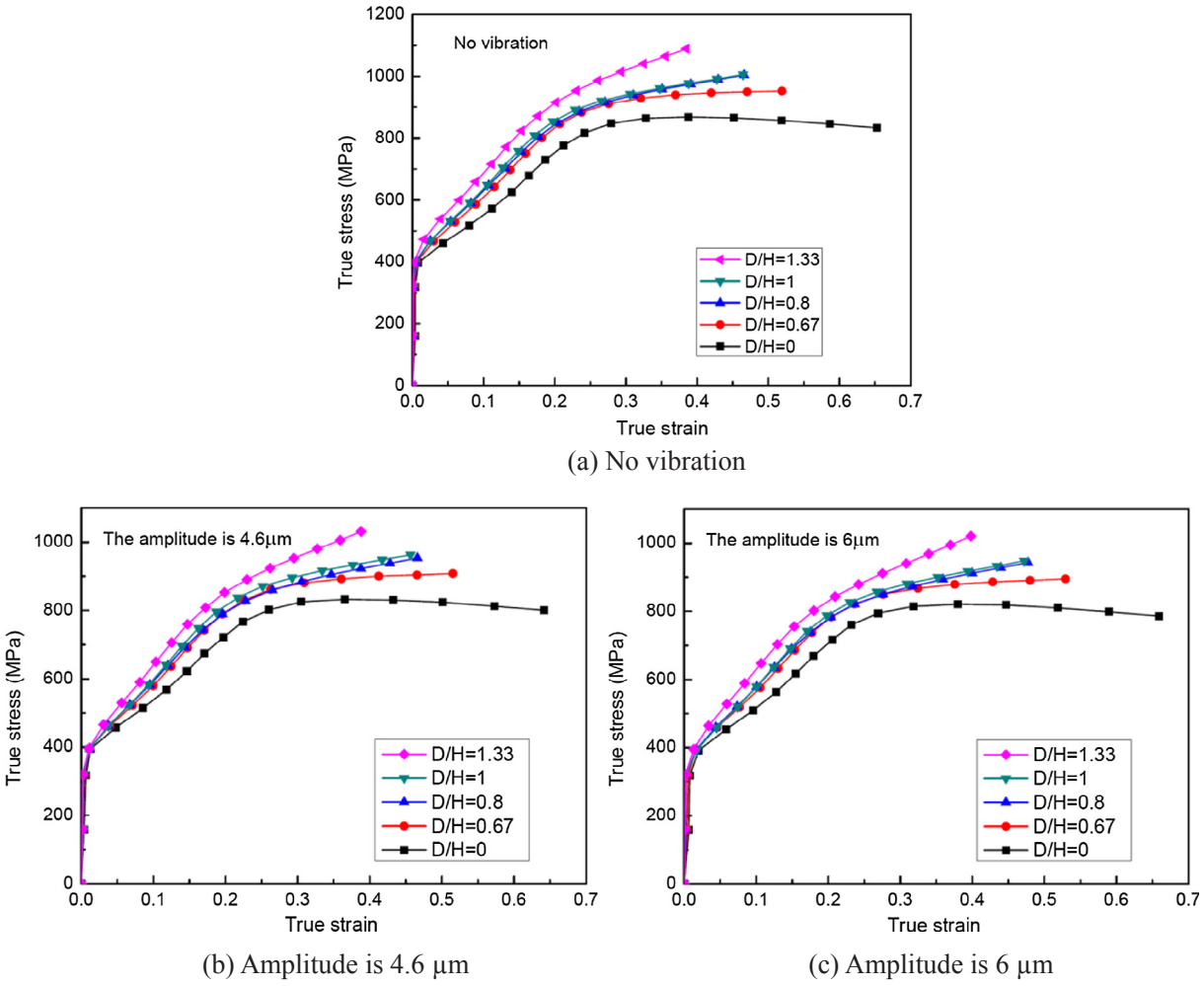

Fig. 7. True stress-strain curves at different D/H ratios.

Table 3
The values of true stress-strain at different vibration loading modes.

Loading modes	No vibration		Amplitude is 4.6 μm		Amplitude is 6 μm	
D/H	1.33	0	1.33	0	1.33	0
True stress (MPa)	1065	845	1031	800	1021	786
True strain	0.35572	0.58656	0.38798	0.64145	0.39807	0.65921

loading modes under frictionless condition, including comparison tests with no vibration, full vibration and intermittent vibration. The amplitudes of full vibration and intermittent vibration are both 4.6 μm in Fig. 10(a). The vibration amplitudes in Fig. 10(b) are 6 μm. From the figures, it showed that the flow stress reduction caused by ultrasonic vibration was same whether the vibration is excited at the beginning or in the middle stage of the compression.

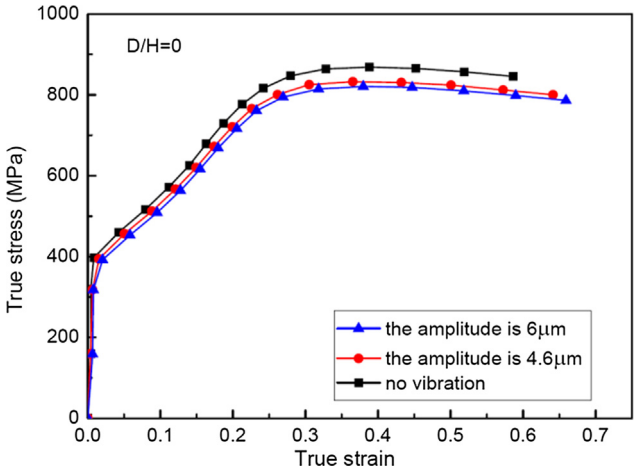

Fig. 8. True stress-strain curves under frictionless condition.

4. Microstructure analysis

In order to study the influence of ultrasonic vibration on the microstructure of the material, the center of the surface of the specimen was observed. First, the specimen was grinded with 400 #, 600 #, 800 #, 1000 # and 1200 # SiC abrasive papers. Grinding started from the 400 # abrasive paper until the surface scratches of the specimen was in the same direction, then the specimen which rotated 90° was grinded with another abrasive paper of higher precision, and repeated the above operation. Second, the grinded specimen was polished on a PG-2B polishing machine until the surface of specimen was bright as a mirror. Finally, the Kroll solution (HF: HNO3: H2O = 3: 5: 100) was used for etching. Fig. 11 represented the microstructure of the annealed specimen which observed under an optical microscope (×200). From the figure, the microstructure of the annealed specimen was uniform and equiaxed, and no twins appear. the grain size was estimated by using the circles cut-off point method in GB/T6394-2017 standard in this

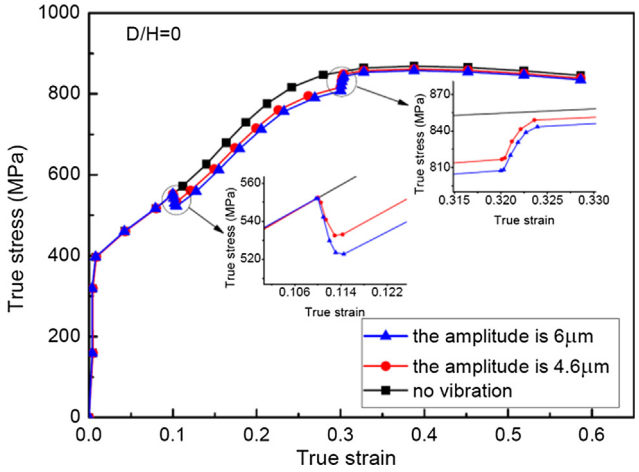

Fig. 9. The true stress-strain curves at different amplitudes for intermittent vibration under frictionless condition.

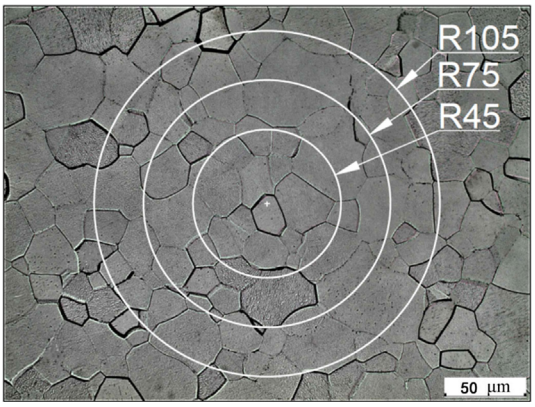

Fig. 11. The microstructure of the annealed specimen.

study, and the original grain size was 22.5 μm. Due to the resolution of the optical microscope is low, and the focusing performance is not good at high magnification, so SEM images was adopted for the analysis of the microstructures subsequently.

Fig. 12 shows the SEM image of specimen with the D/H is 1, compressed with different conditions. Fig. 12(a) is the SEM image of compression without vibration. The amplitudes of Fig. 12(b) and (c) were 4.6 μm and 6 μm respectively. It can be seen from the figure that, in contrast with vibrated compression, a larger amount of deformation twins are generated and the twin orientations are more chaotic in conventional compression, which resulting the material deformation is more difficult to deform. In addition, under the effect of vibration, the reduction of the number of deformation twins could clearly be seen with the amplitude increases. Therefore, under the same strain, the deformation stress in conventional compression is bigger than that in vibrated compression case, which is agreed well with the stress-strain curve in Fig. 8.

The grain size of Fig. 12(a), (b) and (c) were measured to be 12.8 μm, 12.3 μm and 11.7 μm respectively. Deformation twinning is sensitive to the strain rate in the material of titanium, when the strain rate increases, twin mechanism is more likely to be triggered [26]. At low strain stage, the mechanism of slip and twin worked together, while the deformation twins were dominant, and the deformation was difficult [27]. When the vibration is applied, the strain rate of material can reach $368\,s^{-1}$ and $480\,s^{-1}$ corresponding to the vibrations of amplitudes of 4.6 μm and 6 μm, respectively. These high strain rates can promote the generation of twins [28]. In this case, the twins in material would saturate quickly, and then the twin would subdivide the grain, leading to the refinement of the grain and the reduction of the number of twins [29]. At the moment, the deformation is dominant by slippage, and thus the deformation becomes easy [30]. While the deformation twins can also refine the grain in conventional compression, so there is little difference in the grain size when the vibration is applied, but the twins in the specimen decreases under the effect of vibration.

Fig. 13 shows the SEM image of compressive specimen with the D/H is 1 and intermittent vibration. The vibrational interval of Fig. 13(a) and (b) is 0.1 to 0.3 of the strain and the amplitudes are 4.6 μm and 6 μm respectively. It can be seen that when the amplitude is 6 μm, the number of twins is smaller than that when the amplitude is 4.6 μm. Therefore, the resistance of material to deform is smaller in case of 6 μm, so the residual softening of the material is more obvious after the vibration stops, which matches well with the macroscopic phenomenon in Fig. 9.

5. Conclusion

In the present study, the effect of the ultrasonic vibration on the deformation process of pure titanium is focused. In the experiment, the ultrasonic vibration is axially applied on the tool head which compresses the titanium bar with an additional static velocity. By treating and analyzing the experimental data and observing the microstructure, several conclusions can be made as follows:

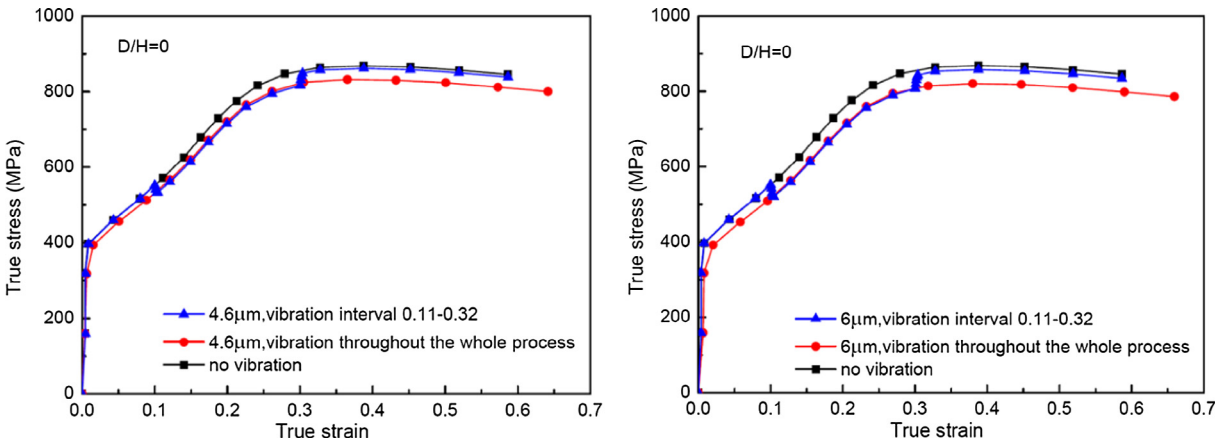

(a) Amplitude is 4.6 μm (a) Amplitude is 6 μm

Fig. 10. The true stress-strain curves of different vibration loading modes under frictionless condition.

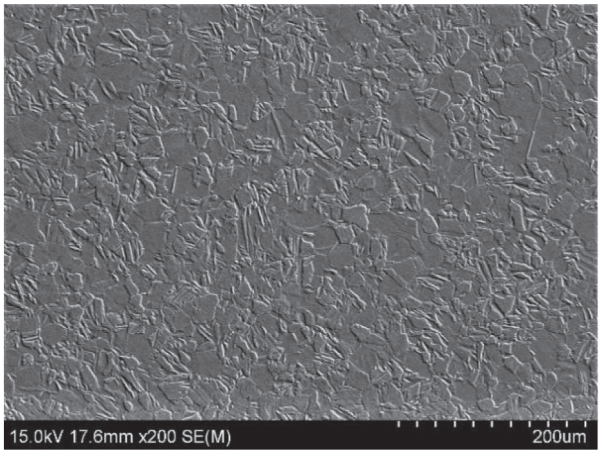

(a) No vibration

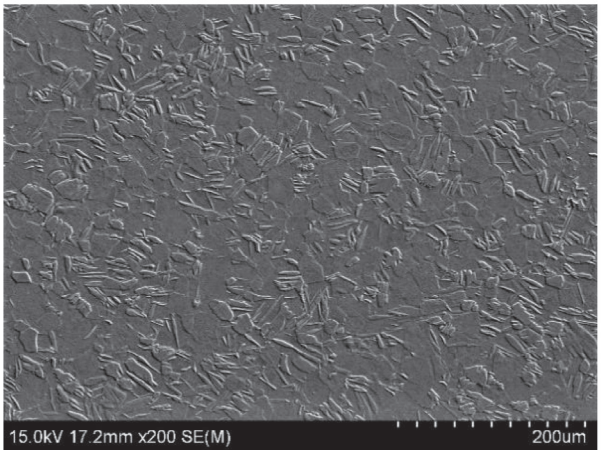

(b) Amplitude is 4.6 μm

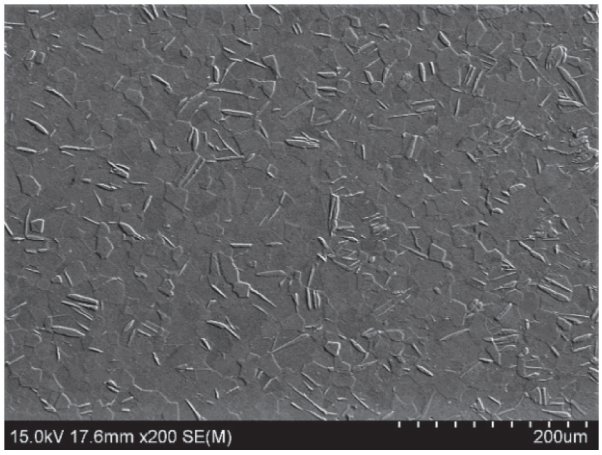

(c) Amplitude is 6 μm

Fig. 12. The SEM image of specimen after the full vibration compression.

(1) The ultrasonic vibration can reduce the yield stress and the flow stress in plastic stage, but has almost no effect on the elastic deformation. In addition, the influence of temperature rising on the test can be ignored.
(2) During ultrasonic vibration assisted pure titanium compression process, the mechanism of the flow stress reduction includes ultrasonic softening, stress superposition and strain hardening under frictionless condition. After stopping vibration in the intermittent vibration process, the material shows a residual softening.
(3) The ultrasonic vibration can promote the generation of the

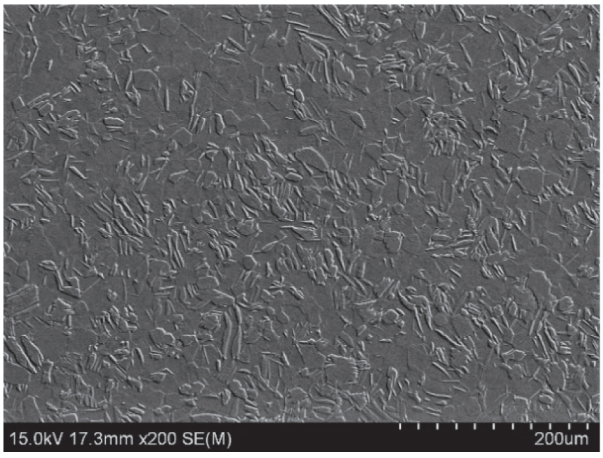

(a) Amplitude is 4.6 μm

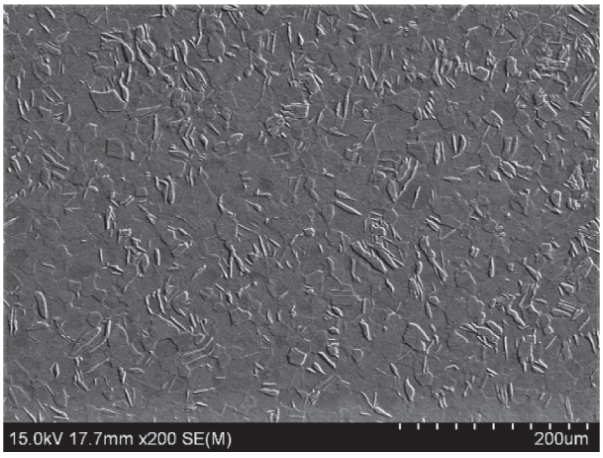

(b) Amplitude is 6 μm

Fig. 13. The SEM image of specimen after the intermittent vibration compression.

deformation twins in the pure titanium and make grain refinement, thus reducing the number of twins.

(4) The residual softening effect is related to the number of deformation twins in pure titanium.

Acknowledgement

This project is supported by National Natural Science Foundation of China (Grant No. 51705291, 51675307, 51375269).

References

[1] G.Z. Luo, R.Z. Liu, Non-aerospace application of Ti materials with a great many social and economic benefits in China, Mater. Sci. Eng. A 280 (2000) 25–29.
[2] F.H. Froes, H. Friedrich, J. Kiese, D. Bergoint, Titanium in the family automobile: the cost challenge, JOM 56 (2004) 40–44.
[3] E. Twohig, P. Tiernan, S.A.M. Tofail, Experimental study on dieless drawing of Nickel-Titanium alloy, J. Mech. Behav. Biomed. Mater. 8 (2012) 8–20.
[4] L.I. Hong-Wei, X.L. Zhang, J.Y. Chen, L.I. Jin-Shan, Effects of stress state on texture and microstructure in cold drawing-bulging of CP-Ti sheet, Trans. Nonferr. Met. Soc. China 23 (2013) 23–31.
[5] E. Teidelt, J. Starcevic, V.L. Popov, Influence of ultrasonic oscillation on static and sliding friction, Tribol. Lett. 48 (2012) 51–62.
[6] A. Siddiq, T. El Sayed, Ultrasonic-assisted manufacturing processes: variational model and numerical simulations, Ultrasonics 52 (2012) 521–529.
[7] F. Blaha, B. Langenecker, Dehnung von Zink-Kristallen unter Ultraschalleinwirkung, Naturwissenschaften 20 (1955) 556-556.
[8] Z. Yao, G.Y. Kima, L.A. Faidley, Q. Zou, D. Mei, Z. Chen, Acoustic softening and residual hardening in aluminum: modeling and experiments, Int. J. Plast. 39 (2012) 75–87.
[9] J.C. Hung, C.C. Lin, Investigations on the material property changes of ultrasonic-vibration assisted aluminum alloy upsetting, Mater. Des. 45 (2013) 412–420.
[10] K. Siegert, J. Ulmer, Superimposing ultrasonic waves on the dies in tube and wire drawing, J. Eng. Mater. Technol. 123 (2001) 517–523.
[11] M. Rasooli, M. Moshref-Javadi, A. Taherizadeh, Investigation of ultrasonic vibration effects on the microstructure and hardness of aluminum alloy 2024 tube spinning parts, Int. J. Adv. Manuf. Technol. 77 (2015) 2117–2124.
[12] S. Amini, A.H. Gollo, H. Paktinat, An investigation of conventional and ultrasonic-assisted incremental forming of annealed AA1050 sheet, Int. J. Adv. Manuf. Technol. 90 (2016) 1–10.
[13] Y. Lou, J.S. He, H. Chen, M. Long, Effects of vibration amplitude and relative grain size on the rheological behavior of copper during ultrasonic-assisted microextrusion, Int. J. Adv. Manuf. Technol. 89 (2017) 2421–2423.
[14] F. Djavanroodi, H. Ahmadian, K. Koohkan, R. Naseri, Ultrasonic assisted-ECAP, Ultrasonics 53 (2013) 1089–1096.
[15] J.C. Hung, Y.C. Tsai, Investigation of the effects of ultrasonic vibration-assisted micro-upsetting on brass, Mater. Sci. Eng. A 580 (2013) 125–132.
[16] V. Fartashvand, A. Abdullah, S.V.S. Ali, Effects of high power ultrasonic vibration on the cold compaction of titanium, Ultrason. Sonochem. 36 (2017) 155–161.
[17] V. Fartashvand, A. Abdullah, S.A. Sadough Vanini, Investigation of Ti-6Al-4V alloy acoustic softening, Ultrason. Sonochem. 38 (2017) 744–749.
[18] C. Yang, X. Shan, T. Xie, Titanium wire drawing with longitudinal-torsional composite ultrasonic vibration, Int. J. Adv. Manuf. Technol. 83 (2016) 645–655.
[19] J. Zhao, Z. Liu, Investigations of ultrasonic frequency effects on surface deformation in rotary ultrasonic roller burnishing Ti-6Al-4V, Mater. Des. 107 (2016) 238–249.
[20] H. Zhou, H. Cui, Q.H. Qin, H. Wang, Y. Shen, A comparative study of mechanical and microstructural characteristics of aluminium and titanium undergoing ultrasonic assisted compression testing, Mater. Sci. Eng. A 682 (2017) 376–388.
[21] Z. Yao, G.Y. Kim, L.A. Faidley, Q. Zou, D. Mei, Z. Chen, Acoustic softening and hardening of aluminum in high-frequency vibration-assisted micro/meso forming, Adv. Manuf. Process. 28 (2013) 584–588.
[22] H.O.K. Kirchner, W.K. Kromp, F.B. Prinz, P. Trimmel, Plastic deformation under simultaneous cyclic and unidirectional loading at low and ultrasonic frequencies, Mater. Sci. Eng. 68 (1985) 197–206.
[23] Z. Yao, G.Y. Kim, L.A. Faidley, Q. Zou, D. Mei, Z. Chen, Effects of superimposed high-frequency vibration on deformation of aluminum in micro/meso-scale upsetting, J. Mater. Process. Technol. 212 (2012) 640–646.
[24] J. Hung, C. Hung, The influence of ultrasonic-vibration on hot upsetting of aluminium alloy, Ultrasonics 43 (2005) 692–698.
[25] M. Cook, E.C. Larke, Resistance of copper and copper alloys to homogeneous deformation in compression, J. Inst. Met. 71 (1945) 371–390.
[26] D.R. Chichili, K.T. Ramesh, K.J. Hemker, The high-strain-rate response of alpha-titanium: experiments, deformation mechanisms and modeling, Acta Mater. 46 (1998) 1025–1043.
[27] A.V. Panin, M.S. Kazachenok, A.I. Kozelskaya, R.R. Hairullin, E.A. Sinyakova, Mechanisms of surface roughening of commercial purity titanium during ultrasonic impact treatment, Mater. Sci. Eng. A 647 (2015) 43–50.
[28] A.I. Dekhtyar, B.N. Mordyuk, D.G. Savvakin, V.I. Bondarchuk, I.V. Moiseeva, N.I. Khripta, Enhanced fatigue behavior of powder metallurgy Ti–6Al–4V alloy by applying ultrasonic impact treatment, Mater. Sci. Eng., A 641 (2015) 348–359.
[29] S. Jelliti, C. Richard, D. Retraint, T. Roland, M. Chemkhi, C. Demangel, Effect of surface nanocrystallization on the corrosion behavior of Ti–6Al–4V titanium alloy, Surf. Coat. Technol. 224 (2013) 82–87.
[30] X. Wu, S.R. Kalidindi, C. Necker, A.A. Salem, Prediction of crystallographic texture evolution and anisotropic stress–strain curves during large plastic strains in high purity α-titanium using a Taylor-type crystal plasticity model, Acta Mater. 55 (2007) 423–432.